Geochemical Perspectives Letters

© 2024 The Authors
Published by the European Association of Geochemistry

Medieval and recent SO_2 budgets in the Reykjanes Peninsula: implication for future hazard

A. Caracciolo, E. Bali, E. Ranta, S.A. Halldórsson, G.H. Guðfinnsson, B.V. Óskarsson

Supplementary Information

The Supplementary Information includes:

- Calculation of SO_2 Emissions
- Modelling Sulfur Degassing
- The Occurrence of Degassed and Partially Degassed Melt Inclusions
- Selection of Enriched and Depleted End Member Melt Compositions
- Modelling SCSS
- Figures S-1 to S-4
- Supplementary Tables S-1 to S-4
- Supplementary Information References

Calculation of SO_2 Emissions

The total mass of sulfur (M_S, [kg]) which was released from the magma and dispersed into the atmosphere can be calculated as:

$$M_S = V_{DRE} \times \rho \times \Delta C_S \,, \qquad \text{(S-1)}$$

where V_{DRE} is the dense rock equivalent volume (vesicle-free) of the erupted lava unit in m^3, ρ is the density of the melt in kg/m^3 and ΔC_S the mass of sulfur release *per* unit mass of melt. Particularly, ΔC_S is calculated as:

$$\Delta C_S = (1 - X)\,(C_{S\,MI} - C_{S\,glass}) \,, \qquad \text{(S-2)}$$

where X is the crystal content of the lava, which is set at 0.02. This is a reasonable and conservative assumption as the 800–1240 AD Fires contain little amount of macrocrysts, <2 vol. % (Caracciolo *et al.*, 2023). $C_{S\,MI}$ and $C_{S\,glass}$ are the pre-eruptive and post-erupted sulfur (S) concentrations for a given eruption, respectively, which in this work were chosen as the maximum and minimum S concentrations measured in MIs and in tephra glasses, respectively (*cf.* Table 1). The volume of the erupted lava unit is expressed as dense rock equivalent (V_{DRE}), which reflects the volume of the vesicle-free lava. However, published lava volumes for the 800–1240

AD Fires refer to bulk volumes and do not take into account the porosity of the lava. For this reason, we estimated V_{DRE} by multiplying the bulk volume (V) for a scaling factor that accounts for vesicularity (0.85 in this work). Due to the lack of vesicularty data for the lava units targeted in this study and considering that vesicularity is highly variable across basaltic lava flows (*e.g.*, Cashman and Kauahikaua, 1997), we use a bulk vesicularity of 15 %, consistent with findings for the 2014–2015 Holuhraun lava flow (Bonny *et al.*, 2018). This bulk vesicularity is within the range of vesicularity constrained for other basaltic lava flows in Iceland, such as Hafnarhraun in the Reykjanes peninsula (12–37 % vesicularity; Nikkola *et al.*, 2019) and Vikrahraun, the 1961 lava flow from Askja (0–30 % vesicularity; Blasizzo *et al.*, 2022).

Assessing the daily SO_2 emissions of past eruptions is challenging, particularly for those eruptions where the duration is unknown, such as for the 800–1240 AD Fires. We calculated daily SO_2 emissions [kg/d] starting from MOR values using the following equation:

$$\text{Daily } SO_2 \text{ emissions} = \text{MOR}_i \times \rho \times (\Delta C_S \times 2) \times 86{,}400 \text{ . (S-3)}$$

Additionally, in Table 1 we included the amount of time required to erupt and emplace a specific volume of magma, which can be used as a proxy for eruption durations. We call this time of lava emplacement. In fact, we cannot rule out that erupted volumes reflect multiple eruptive phases over which the lava was emplaced, as observed during the 2023–2024 Svartsengi eruptions (<48 h) and as suggested by Caracciolo *et al.* (2023). The time of lava emplacement (t_m [days]) of each eruptive unit was calculated by using MOR values calculated by Óskarsson *et al.* (2024) (Table 1), using the following equation:

$$t_m = \frac{V_i}{\text{MOR}_i \times 86{,}400}, \qquad \text{(S-4)}$$

where V_i [m^3] and MOR_i [m^3/s] are the bulk volume and the MOR of a specific lava unit, respectively. The time of lava emplacement for the new 2021–2024 eruptions at Fagradalsfjall and Svartsengi represents the actual duration of each eruption. Óskarsson *et al.* (2024) calculate mean output rates (MOR) and uncertainty ranges for each eruption targeted in this work. Therefore, the time of lava emplacement and daily SO_2 emissions for each eruption was calculated taking into account the uncertainty range in MOR values (Table 1).

Modelling Sulfur Degassing

Sulfur degassing was modelled using the open source COHS-degassing model Sulfur_X (Ding *et al.*, 2023), using the COH model of Newman and Lowenstern (2002) and the S speciation model of O'Neill and Mavrogenes (2022). Oxygen fugacity was set at ΔFMQ = 0 (Novella *et al.*, 2020) and T = 1200 °C. Pre-eruptive S concentration was chosen as 1550 ppm based on MI data, whereas H_2O and CO_2 concentrations were estimated at 0.3 wt. % and 1000 ppm, respectively, in agreement with typical H_2O and CO_2 concentrations of Icelandic rift basalts (*e.g.*, Bali *et al.*, 2018; Halldórsson *et al.*, 2022). Melt composition was chosen as the mean groundmass glass compositions of the 800–1240 AD Fires. We also tested S degassing of hypothetical scenarios with higher melt H_2O contents of 1.5 wt. % and 3 wt. %, unrealistically high for Iceland rift basalts (Ranta *et al.*, 2024). Higher H_2O contents push the onset of S degassing to higher pressures.

However, >3 wt. % H_2O contents are required for significant S degassing to occur at known magma storage depths.

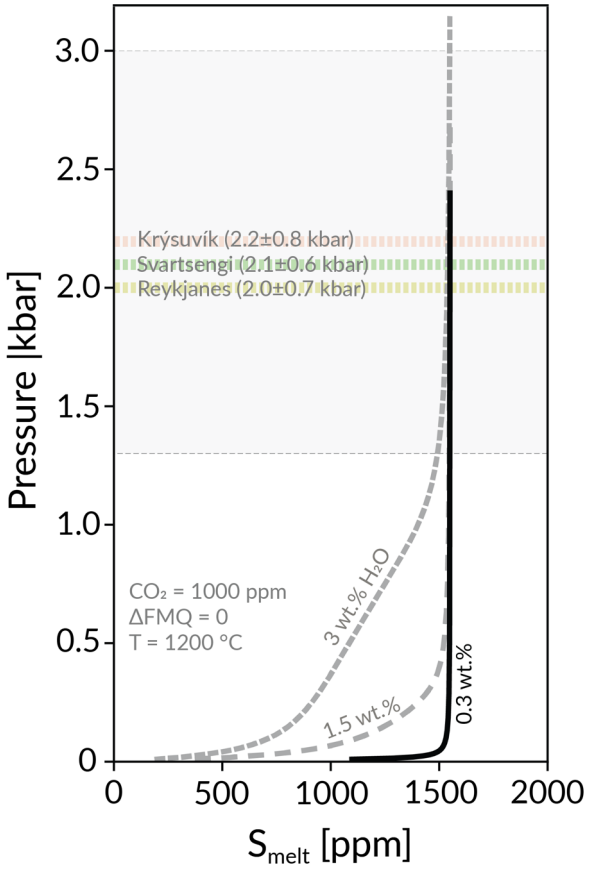

Figure S-1 Models of melt S degassing as a function of pressure. Thick black curve indicates realistic H_2O contents for Reykjanes basalts. Dashed grey lines indicate S degassing assuming unrealistically high H_2O contents of 1.5 and 3 wt. %. Modelling was carried out using Sulfur_X (Ding *et al.*, 2023).

The Occurrence of Degassed and Partially Degassed Melt Inclusions

Many melt inclusion compositions from Brennisteinsfjöll, and to a lesser extent, from Svartsengi, are found to be partially to fully degassed (Fig. 1). In the case of Brennisteinsfjöll, in which we have a larger amount of partially and fully degassed MIs, individual crystals contain multiple MIs with variable S contents. Within the same crystal, some MIs have 'normal' S contents (>1200 ppm) consistent with fractional crystallisation trends, whereas some are partially (400–1100 ppm S) degassed (Fig. 1). Additionally, some MIs are completely degassed, with S contents similar to groundmass values (<400 ppm) (Fig. 1d). Based on backscattered electron (BSE) images, those MIs that are partially to completely degassed contain very large bubbles (Fig. S-2). Post-entrapment degassing at low-*P* (*e.g.*, during eruption) could be responsible for the observed partially to completely degassed MIs in Brennisteinsfjöll. The MIs could release S at low pressure, such as when a host

crystal fractures during an eruption, causing the pressure within certain MIs to rapidly decrease to nearly atmospheric. In this scenario, the melt within the MIs degasses sulfur into the shrinkage bubble prior to quenching.

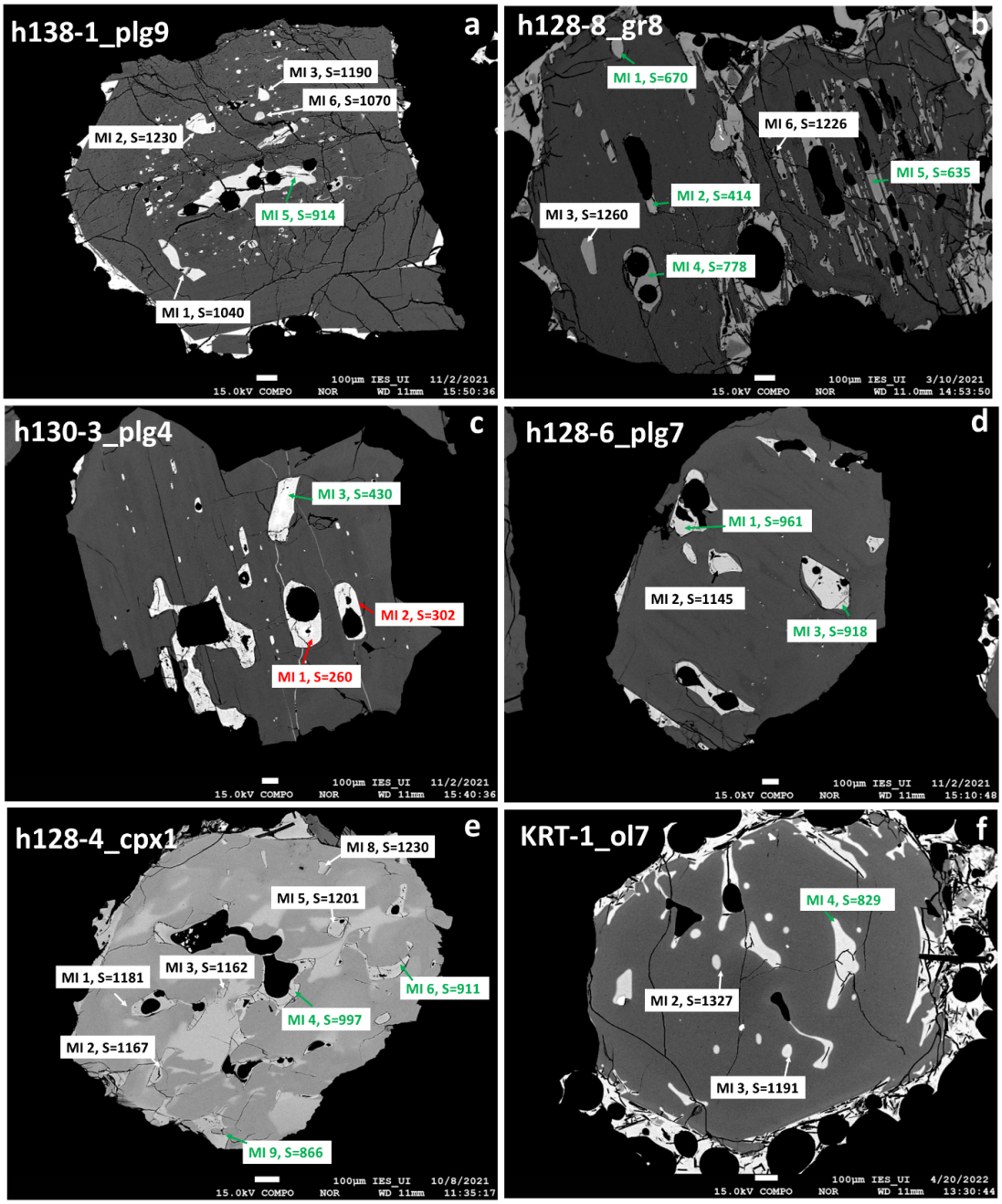

Figure S-2 BSE images of **(a–d)** plagioclase, **(e)** clinopyroxene and **(f)** olivine crystals from Brennisteinsfjöll containing multiple MIs with different S contents. Note that partially and completely degassed MIs contain large bubbles, which probably contained S-bearing mineral precipitates which sequestered a significant amount of S.

Selection of Enriched and Depleted End Member Melt Compositions

End member melt compositions were selected from the MI record preserved in the 800–1240 AD Fires and using K_2O/TiO_2 as a proxy for magma enrichment, which has been proven to be a robust tracer of mantle-derived chemical variability (Halldórsson *et al.*, 2022; Harðardóttir *et al.*, 2022). For the depleted end member melt composition, the MI dataset was filtered by selecting and averaging PEP-corrected MI compositions (n = 3) satisfying the following criteria: $K_2O/TiO_2 < 0.1$, Mg# > 70 and MgO > 9 wt. %. The resulting melt composition has Mg# = 70.4, 9.5 wt. % MgO and S content of 680 ± 85 ppm. The enriched end member melt composition was chosen by averaging MI compositions (n = 4) satisfying the following criteria: Mg# > 69, MgO > 9 wt. %, $K_2O/TiO_2 > 0.3$ and $TiO_2 > 0.4$ wt. %. The resulting composition has Mg# = 70, 9.8 wt. % MgO and S content of 872 ± 166 ppm. Starting from these initial compositions, we modelled fractional crystallisation using Petrolog3 (Danyushevsky and Plechov, 2011) at 2 kbar and at fO_2 corresponding to the FMQ buffer. S partition coefficient between melt and olivine, plagioclase and clinopyroxene were taken from Callegaro *et al.* (2020) (S partition coefficient of Cpx–melt = 0.05, Olivine–melt = 0.01, Plagioclase–melt = 0.13).

Modelling SCSS

Sulfur concentration at sulfide saturation (SCSS) was modelled along an empirical fractional crystallisation path calculated between Mg# = 75 and Mg# = 40 by regressing the observed MI and glass data with linear functions for each volcanic system. Melt temperature was calculated using the melt-only thermometer (Eq. 14 in Putirka, 2008). SCSS modelling was implemented in PySulfSat (Wieser and Gleeson, 2022), by comparing different SCSS models (Fortin *et al.*, 2015; Smythe *et al.*, 2017; O'Neill and Mavrogenes, 2022) (Fig. S-2). For the modelling parameters, we used $Fe^{3+}/Fe^{tot} = 0.1$, P = 2 kbar and sulfide Fe/(Fe+Ni+Cu) = 0.65. The different models yield similar results and well within the 1σ uncertainty of the Smythe *et al.* (2017) model (see Fig. S-3a–d).

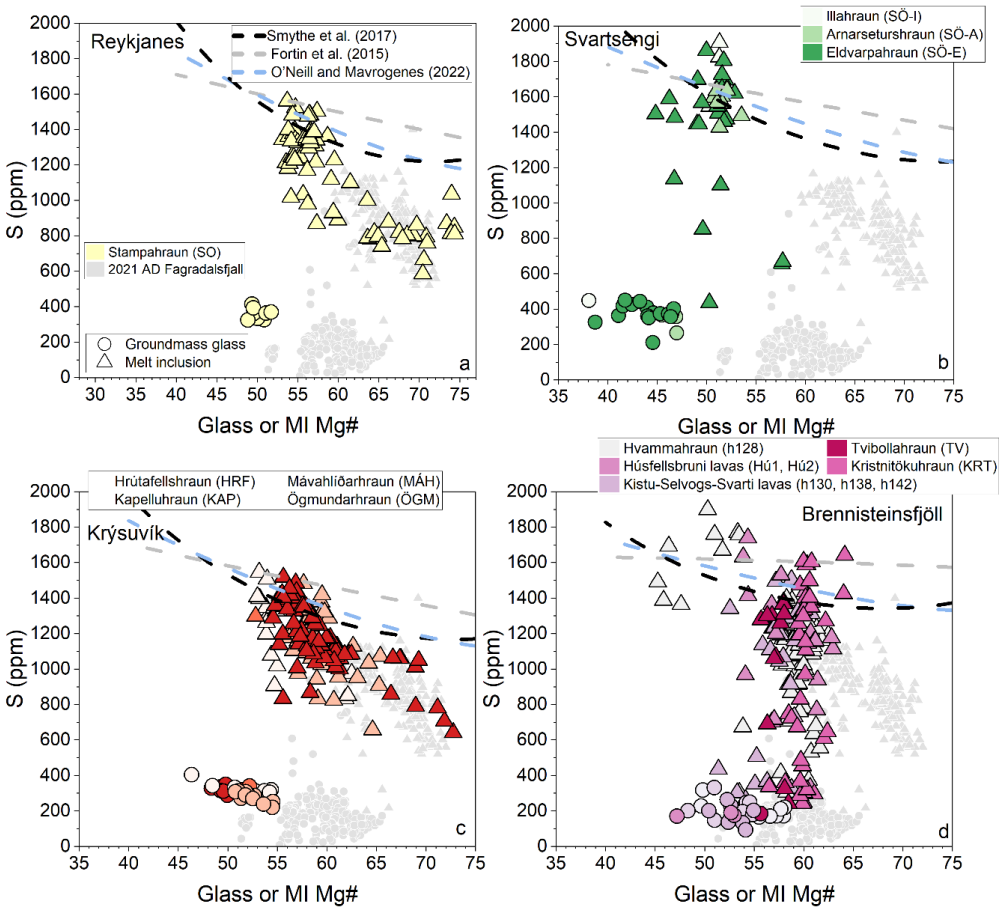

Figure S-3 Variation of S contents in groundmass glasses (filled circles) and PEP-corrected MIs (filled triangles) as a function of Mg# in samples from the 800–1240 AD Fires and the 2021 Fagradalsfjall eruption. The purpose of the figure is to compare results from different SCSS models, indicated with different dashed curves.

Figure S-4 [next page] **(a–d)** Variation of S contents in groundmass glasses (filled circles) and PEP-corrected MIs (filled triangles) as a function of Mg# [Mg# = 100·Mg/(Mg+Fe^{2+}), Fe^{2+}/Fe^{tot} = 0.9] in samples from the 800–1240 AD Fires and raw MI data from the December 2023, January 2024 and February 2024 Sundhnúkuar eruptions. Data from the 2021 AD Fagradalsfjall eruption are from Halldórsson *et al*. (2022). Red and blue solid lines indicate fractional crystallisation paths calculated for a geochemically enriched and depleted initial melt compositions, respectively. The black dashed curve indicates SCSS along an empirical fractional crystallisation path calculated after Smythe *et al.* (2017). **(e–h)** Measured MI S contents *vs*. calculated SCSS, coloured after MgO content. SCSS was calculated assuming Fe^{3+}/Fe^{tot} = 0.1, P = 2 kbar, T = 1220 °C and sulfide Fe/(Fe+Ni+Cu) = 0.65, after the method of Smythe *et al*. (2017) (*cf*. Fig. S-3). All SCSS models were implemented in PySulfSat code (Wieser and Gleeson, 2022).

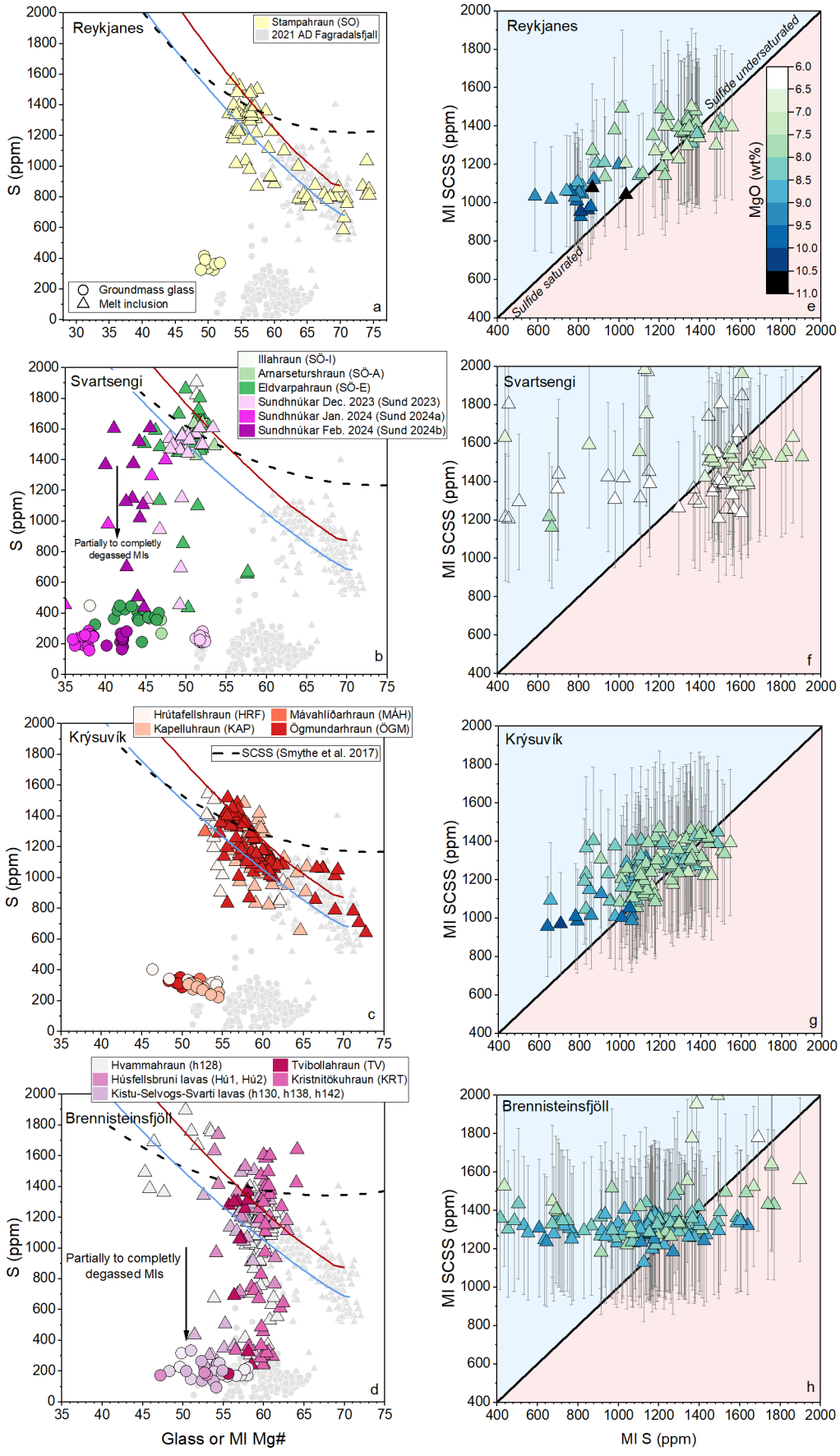
Reykjanes
Stampahraun (SO)
2021 AD Fagradalsfjall
Groundmass glass
Melt inclusion
a
Svartsengi
Illahraun (SÖ-I)
Arnarseturshraun (SÖ-A)
Eldvarpahraun (SÖ-E)
Sundhnúkar Dec. 2023 (Sund 2023)
Sundhnúkar Jan. 2024 (Sund 2024a)
Sundhnúkar Feb. 2024 (Sund 2024b)
Partially to completly degassed MIs
b
Krýsuvík
Hrútafellshraun (HRF)
Kapelluhraun (KAP)
Mávahlíðarhraun (MÁH)
Ögmundarhraun (ÖGM)
SCSS (Smythe et al. 2017)
c
Brennisteinsfjöll
Hvammahraun (h128)
Húsfellsbruni lavas (Hú1, Hú2)
Kistu-Selvogs-Svarti lavas (h130, h138, h142)
Tvíbollahraun (TV)
Kristnitökuhraun (KRT)
Partially to completly degassed MIs
d
S (ppm)
Glass or MI Mg#
Reykjanes
Sulfide undersaturated
Sulfide saturated
MgO (wt%)
e
Svartsengi
f
Krýsuvík
g
Brennisteinsfjöll
h
MI SCSS (ppm)
MI S (ppm)

Supplementary Tables

The MI and glass dataset published in this work complement the dataset published in Caracciolo *et al*. (2023) and here includes S and Cl measurements. Re-homogenized melt inclusions are not included in this work. Additionally, the dataset includes new groundmass and MI data from the data from the 2022–2023 Fagradalsfjall eruptions and the 2023–2024 eruptions at Sundhnúksgígar in Svartsengi.

Table S-1 Overview of samples studied in this work, along with acronyms, lava flows, ages and coordinates. Analysed phases in each sample are indicated with cross marks.

Table S-2 Groundmass glass dataset.

Table S-3 Mean compositions of groundmass glasses and glass standards.

Table S-4 Melt inclusion dataset listing PEP-corrected and raw compositions, along with host mineral compositions and 1σ uncertanties. Note that MIs from the 2023 Fagradalsfjall eruption and the December 2023 and January 2024 Sundhnúksgígar eruptions have not been PEP-corrected.

Tables S-1 to S-4 are available for download (.xlsx) from the online version of this article at http://doi.org/10.7185/geochemlet.2417.

Supplementary Information References

Bali, E., Hartley, M.E., Halldórsson, S.A., Gudfinnsson, G.H., Jakobsson, S. (2018) Melt inclusion constraints on volatile systematics and degassing history of the 2014–2015 Holuhraun eruption, Iceland. *Contributions to Mineralogy and Petrology* 173, 9. https://doi.org/10.1007/s00410-017-1434-1

Blasizzo, A.Y., Ukstins, I.A., Scheidt, S.P., Graettinger, A.H., Peate, D.W., Carley, T.L., Moritz, A.J., Thines, J.E. (2022) Vikrahraun—the 1961 basaltic lava flow eruption at Askja, Iceland: morphology, geochemistry, and planetary analogs. *Earth, Planets and Space* 74, 168. https://doi.org/10.1186/s40623-022-01711-5

Bonny, E., Thordarson, T., Wright, R., Höskuldsson, A., Jónsdóttir, I. (2018) The Volume of Lava Erupted During the 2014 to 2015 Eruption at Holuhraun, Iceland: A Comparison Between Satellite- and Ground-Based Measurements. *Journal of Geophysical Research: Solid Earth* 123, 5412–5426. https://doi.org/10.1029/2017JB015008

Callegaro, S., Geraki, K., Marzoli, A., de Min, A., Maneta, V., Baker, D.R. (2020) The quintet completed: The partitioning of sulfur between nominally volatile-free minerals and silicate melts. *American Mineralogist* 105, 697–707. https://doi.org/10.2138/am-2020-7188

Caracciolo, A., Bali, E., Halldórsson, S.A., Guðfinnsson, G.H., Kahl, M., Þórðardóttir, I., Pálmadóttir, G.L., Silvestri, V. (2023) Magma plumbing architectures and timescales of magmatic processes during

historical magmatism on the Reykjanes Peninsula, Iceland. *Earth and Planetary Science Letters* 621, 118378. https://doi.org/10.1016/j.epsl.2023.118378

Cashman, K.V., Kauahikaua, J.P. (1997) Reevaluation of vesicle distributions in basaltic lava flows. *Geology* 25, 419–422. https://doi.org/10.1130/0091-7613(1997)025<0419:ROVDIB>2.3.CO;2

Danyushevsky, L.V., Plechov, P. (2011) Petrolog3: Integrated software for modeling crystallization processes. *Geochemistry, Geophysics, Geosystems* 12, Q07021. https://doi.org/10.1029/2011GC003516

Ding, S., Plank, T., Wallace, P.J., Rasmussen, D.J. (2023) Sulfur_X: A Model of Sulfur Degassing During Magma Ascent. *Geochemistry, Geophysics, Geosystems* 24, e2022GC010552. https://doi.org/10.1029/2022GC010552

Fortin, M.-A., Riddle, J., Desjardins-Langlais, Y., Baker, D.R. (2015) The effect of water on the sulfur concentration at sulfide saturation (SCSS) in natural melts. *Geochimica et Cosmochimica Acta* 160, 100–116. https://doi.org/10.1016/j.gca.2015.03.022

Halldórsson, S.A., Marshall, E.W., Caracciolo, A., Matthews, S., Bali, E., Rasmussen, M.B., Ranta, E., Robin, J.G., Guðfinnsson, G.H., Sigmarsson, O., Maclennan, J., Jackson, M.G., Whitehouse, M.J., Jeon, H., van der Meer, Q.H.A., Mibei, G.K., Kalliokoski, M.H., Repczynska, M.M., Rúnarsdóttir, R.H., Sigurðsson, G., Pfeffer, M.A., Scott, S.W., Kjartansdóttir, R., Kleine, B.I., Oppenheimer, C., Aiuppa, A., Ilyinskaya, E., Bitetto, M., Giudice, G., Stefánsson, A. (2022) Rapid shifting of a deep magmatic source at Fagradalsfjall volcano, Iceland. *Nature* 609, 529–534. https://doi.org/10.1038/s41586-022-04981-x

Harðardóttir, S., Matthews, S., Halldórsson, S.A., Jackson, M.G. (2022) Spatial distribution and geochemical characterization of Icelandic mantle end-members: Implications for plume geometry and melting processes. *Chemical Geology* 604, 120930. https://doi.org/10.1016/j.chemgeo.2022.120930

Newman, S., Lowenstern, J.B. (2002) VolatileCalc: a silicate melt–H_2O–CO_2 solution model written in Visual Basic for excel. *Computers & Geosciences* 28, 597–604. https://doi.org/doi:10.1016/S0098-3004(01)00081-4

Nikkola, P., Thordarson, T., Rämö, O.T., Heikkilä, P. (2019) Formation of segregation structures in Hafnarhraun pāhoehoe lobe, SW Iceland: a window into crystal–melt separation in basaltic magma. *Bulletin of Volcanology* 81, 70. https://doi.org/10.1007/s00445-019-1330-9

Novella, D., Maclennan, J., Shorttle, O., Prytulak, J., Murton, B.J. (2020) A multi-proxy investigation of mantle oxygen fugacity along the Reykjanes Ridge. *Earth and Planetary Science Letters* 531, 115973. https://doi.org/10.1016/j.epsl.2019.115973

O'Neill, H.St.C., Mavrogenes, J.A. (2022) The sulfate capacities of silicate melts. *Geochimica et Cosmochimica Acta* 334, 368–382. https://doi.org/10.1016/j.gca.2022.06.020

Óskarsson, B.V. , Askew, R.A., Guðmundsson, H. (2024) Assessing the mean output rate (MOR) of past effusive basaltic eruptions - a look at the postglacial volcanism of the Reykjanes Peninsula in Iceland. *EarthArXiv* Preprint v1. https://doi.org/10.31223/X5CH68

Putirka, K.D. (2008) Thermometers and Barometers for Volcanic Systems. *Reviews in Mineralogy and Geochemistry* 69, 61–120. https://doi.org/10.2138/rmg.2008.69.3

Ranta, E., Halldórsson, S.A., Óladóttir, B.A., Pfeffer, M.A., Caracciolo, A., Bali, E., Guðfinnsson, G.H., Kahl, M., Barsotti, S. (2024) Magmatic Controls on Volcanic Sulfur Emissions at the Iceland Hotspot. *EarthArXiv* Preprint v1. https://doi.org/10.31223/X51102

Smythe, D.J., Wood, B.J., Kiseeva, E.S. (2017) The S content of silicate melts at sulfide saturation: New experiments and a model incorporating the effects of sulfide composition. *American Mineralogist* 102, 795–803. https://doi.org/10.2138/am-2017-5800CCBY

Wieser, P.E., Gleeson, M. (2022) PySulfSat: An open-source Python3 tool for modeling sulfide and sulfate saturation. *Volcanica* 6, 107–127. https://doi.org/10.30909/vol.06.01.107127